

Droplet Manipulation and Colloidal Particle Self-assembling in Space



Yuren Wang, Ding Lan and Weibin Li

Abstract The manipulation of liquid drops could be very promising in space applications, such as fluid management, heat exchangers, life support systems, etc. Colloidal material box is one of a subsystem and payload of SJ-10 satellite, which was designed for studying the aqueous drop control and colloidal assembling in space. Based on space experiment platform (colloid material box), we have carried out the drop manipulation experiment in space successfully by using the hydrophilic/hydrophobic patterned surface technique, and the mechanism of the drop wetting and control on the patterned substrate during drop evaporation have been further studied. In addition, the drying process of the constrained colloidal drops on the patterned surface has been investigated. Through analyzing deposition patterns of both sessile and pendant droplets, we found that the deposition morphology is the result of competition and cooperation interactions of the free setting, the interface shrinkage and the outward capillary flow. Two different regimes for the relative motion between the particles and the interface was proposed: the pursuit regime (sessile droplet) and the meeting regime (pendant droplet), which furthered the theory of particles deposition in drying droplet.

Keywords Complex fluids · Drop manipulation · Colloidal assembling · Deposition patterns · Evaporation

Y. Wang (✉) · D. Lan · W. Li

Key Laboratory of Microgravity (National Microgravity Laboratory), Institute of Mechanics, Chinese Academy of Sciences, No. 15 Beisihuanxi Road, Haidian District, Beijing 100190, China
e-mail: yurenwang@imech.ac.cn

School of Engineering Science, University of Chinese Academy of Sciences, No. 19(A) Yuquan Road, Shijingshan District, Beijing 100049, China

© Science Press and Springer Nature Singapore Pte Ltd. 2019
W. R. Hu and Q. Kang (eds.), *Physical Science Under Microgravity: Experiments on Board the SJ-10 Recoverable Satellite*, Research for Development,
https://doi.org/10.1007/978-981-13-1340-0_6

1 Introduction

In this chapter, we focused on the droplet manipulation and colloidal particle self-assembling in space. Gravity driven flow is naturally occurred on earth and is utilized to manipulate fluid flow in abundant applications in industry. However, this privilege is no longer possessed in space. In space, absence of gravity induced surface tension gradient and capillary force dominating the fluid flow. Under this circumstance, a lot of work has been done aimed at solving fluid transport in microgravity. In the last two decades, most of studies in this field concentrated on controlling large volume fluid in space, such as fuel transport in the fuel tank. Recently, the studies turn to concern controlling small volume liquid transport inside experimental and life support system, such as droplet movements in an open cabin and liquid–liquid separation in spacecraft. It is of vital significance for human beings long-term staying in space. In 2017, several space experiments on the study of surface tension measurement and control were done in ISS, including “Surface Tension Containment Experiment-1”, “Capillary Structures for Exploration Life Support” and “Continuous Liquid–Liquid Separation in Microgravity”.

This chapter was divided into five parts. In Sect. 2, we introduced the Colloidal Material Box (CMB) facility boarding SJ-10 recoverable satellite. Section 3 focused on the water and colloidal droplets manipulation technique and the evaporation processes in an open space cabin. Subsequently, the colloidal self-assembling physics in the evaporation process of colloidal droplets was described in Sect. 4. Conclusion and outlook were summarized in the final part.

2 The First Attempt for the Colloidal Assembly in the Space

Colloidal system is an ideal model to study phase transitions and defect formation [1], because in comparison to atoms, micron-sized colloidal particles are big enough and move sufficiently slowly to allow direct observation with optical microscopy, thus the phase change and defect formation processes on the “atomic” scale could be visualized [2]. However, due to the gravity, the colloidal particles will sediment and result in uneven concentrations of colloidal system. It will be difficult to accurately distinguish the relationship between the phase transition and the precipitate [3].

Convective assembly is a widely adopted method to form ordered structure in the colloidal suspension [4]. A template assisted self-assembly (TASA) method was developed by Xia and Yin, which was used to produce a variety of complex aggregates with well-controlled sizes, shapes and structures [5]. More recently, D.J. Norris explored the properties of photonic crystals by self-assembly from colloidal microspheres, and found that solvent flow played a critical role in controlling the formation process [6]. Convective assembly relies on the accumulation of particles near three phase contact lines driven by solvent evaporation, which was attributed to capillary flow resulting from non-uniform evaporation flux and contact

line pinning [7]. However, when the convective process induced by evaporation occurs at ground-level, the self-assembling behavior is obscured by gravitational effects including sedimentation and buoyancy convection, and particles are assembled in every desired orientation to the gravitational vector [8, 9]. Under microgravity conditions, the self-assembly process induced by evaporation occurs in a uniform environment that is devoid of gravity-driven, deleterious convective mass transport or sedimentation effects [10]. Therefore, the change to a gravity-free environment is expected to have a remarkable effect on the assembly dynamics and final deposition patterns.

As a colloidal suspension, the phase transition process of liquid crystal is affected by parameters such as gravity, diffusion force and particle dispersion, but the details of these effects remain unclear [11]. A theory was formulated to describe the mechanism of phase transition in liquid crystal [12], hypothesizing that the liquid crystal phase transition is an entropy-driven process based on the results of competition, interaction of the excluded volume, and orientational entropy [13]. Onsager theory assumed that the phase transition was an ideal process without consideration of effects of gravity. However, due to the presence of gravity, the diffusion force, polydispersity of particles and long-range interactions between molecules on the ground, the actual phase transition likely differs from the ideal process. Thus, it is important to verify and correct Onsager theory in microgravity conditions.

Most research demonstrated that gravity plays a prominent role in affecting the structure of colloidal crystals and the phase transition process of colloidal suspensions [14, 15]. The phase behavior of colloidal particles under microgravity conditions has been studied, and experimental results have also been obtained from space research, including nucleation and growth processes in colloidal crystallization [16, 17], kinetics of colloidal alloy crystallization of binary mixtures [18, 19], and heterogeneous nucleation induced by seed or wall [20]. The positive influence of gravity on the self-assembly and crystal-growth processes was detected [10]. Further study of these processes should be performed as space experiments. The recoverable satellite is an effective tool for space experiments in the microgravity environment [21, 22], and many space microgravity experiments in China have been completed aboard recoverable satellites since the late 1980s. In the mid-2000s, the Chinese National Space Administration (CNSA) developed SJ-10 recoverable satellites, which were mainly used to perform experiments of microgravity science and space life science. The engineering phase of program SJ-10 was started by Chinese Academy of Sciences (CAS) since the beginning of 2013, and the satellite was launched in early 2016 [23], and stayed for 15 days in Earth orbit. The colloidal material box (CMB) is one of several experimental boxes aboard the SJ-10 satellite, which was used to study the self-assembly dynamics of the colloidal spheres (with or without Au-coated nanoparticles) under microgravity, and to test the liquid crystal phase transition model, namely the Onsager model in space.

2.1 The Structure and Functional Units of the Colloidal Material Box (CMB)

The structure and function of the CMB which consists of three modules: (i) Colloidal evaporation experimental module, made up of a sample management unit, an injection management unit, and an optical observation unit, using to observe the self-assembly process of colloidal spheres at the solid/liquid interface and the change of the droplet profile under microgravity. (ii) Liquid crystal phase transition experiments module, including a sample management unit and an optical observation unit, to observe the process of liquid crystal phase transition and verify the mechanism of phase formation driven by entropy alone. (iii) Electronic control module, to manage the experimental procedure in Earth orbit and respond to interface of the integrated electrical control box on the satellite.

Two experimental projects to be implemented in space are listed in Table 2 of Chap. 1 (i) Self-assembly of colloidal spheres induced by evaporation. As shown in Fig. 1, five colloidal drops with different volumes will be injected in sequence onto the five sample positions installed on the linear displacement platform. The change of colloidal droplet profile with evaporation will be recorded by CCD1 camera, capturing side-view images at 0.5 fps. These images will be used to calculate the apparent contact angle, volume, radius, and height of the droplet. The time-dependent contact angle of the droplet will be obtained. In addition, the dynamic deposition process of colloidal microspheres during evaporation will be captured by CCD2 camera at 5 fps, in which continual microscopic images will reveal the movement direction and deposition rate of the particles at the solid/liquid interface during droplet evaporation. We will also obtain images of ordered and disorder phases of the final deposition by moving the linear displacement platform. (ii) Formation and evolution process of ordered phase driven by entropy alone. Six liquid crystal samples of different concentrations will be put in the sample positions within the analyzer and polarizer as shown in Fig. 1. We will observe the phase transition process using CCD3 camera, and obtain color macroscopic images of the liquid crystal phase transition at 30-min intervals. From the images, we will observe the morphology of ordered phase with different concentrations, analyze the liquid crystal orientation, and obtain the phase transformation time.

2.2 Colloidal Evaporation Experimental Module of the CMB

The CMB includes three parts as shown in Fig. 2. (i) Colloidal evaporation experimental module, composed of a sample management unit, an injection management unit, and an optical observation unit. (ii) Liquid crystal phase transition experimental module, which consists of a sample management unit and an optical observation unit. (iii) Electronic control module, to manage the experimental procedure of the first two modules and respond to the interface of the integrated electrical control box located

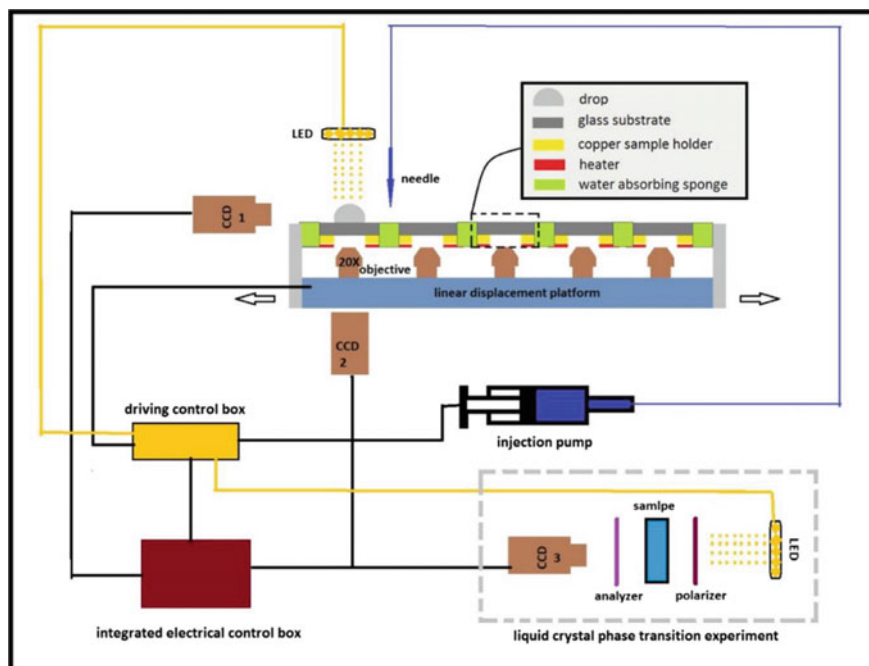


Fig. 1 Experimental principle diagram of the CMB, reprinted from Ref. [24], copyright 2016, with permission from Springer

in the instrument compartment on the SJ-10 satellite, allowing image acquisition and transmission.

The sample management unit was designed to provide sample positions necessary for a drop evaporation experiment, heating the samples, and implementing conversion of the sample positions. The optical observation unit will be used to observe the outer droplet profile and the motion of colloidal particles within the droplet during evaporation. These two units were integrated in the colloidal experimental table as shown in Fig. 3a.

There are five colloidal sample positions with sample substrates, one motor, a linear displacement platform, sets of parts for sample heating and a thermal sensor (DS18B20), five microscope objectives, one deflective optical path, and two CCDs. The motor can move the linear displacement platform back and forth linearly, and the five sample positions can be switched sequentially. Figure 3b shows that each sample position has a heating plate. The heating range can be controlled between 40 and 55 degrees Celsius, and the stability of temperature control is less than 1 degrees Celsius. The thermal sensor (DS18B20) contacting the sample substrate is used for temperature acquisition.

The five microscopic objectives were fixed on the linear displacement platform, and each of them was placed just below the sample position, so they could move

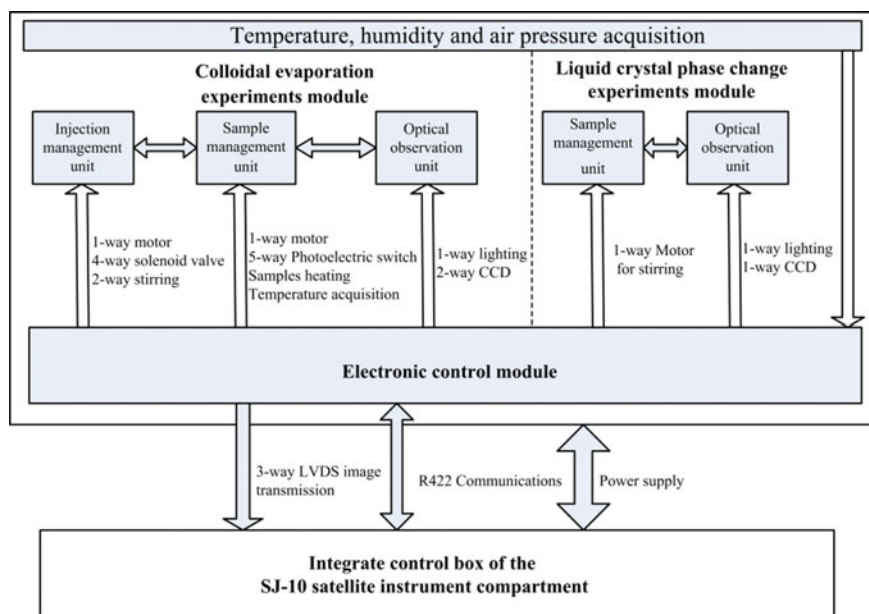


Fig. 2 Flow chart of composition and application of the CMB, reprinted from Ref. [24], copyright 2016, with permission from Springer

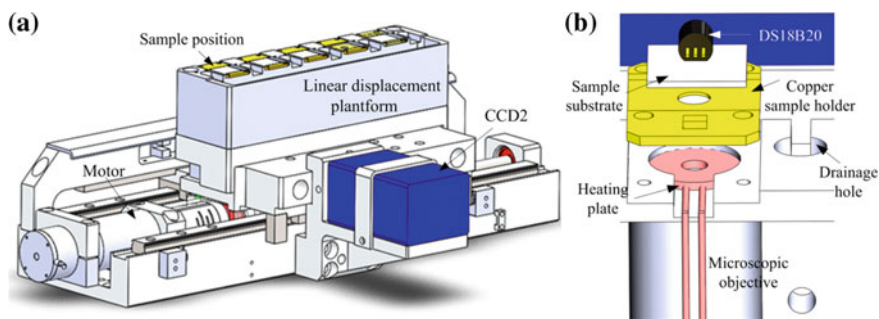


Fig. 3 **a** Schematic of colloidal experiments table; **b** The schematic of the structure of a colloidal sample position on the experimental table. Reprinted from Ref. [24], copyright 2016, with permission from Springer

synchronously with displacement of the platform (Fig. 3b). CCD2 was fixed on the experimental table, which allows observation of microscopic images in the corresponding sample position by deflective optical path, the hole for positioning the optical path, and the axis of CCD2. The side-view CCD (CCD1) was fixed for macroscopic observation of the droplet profile, as shown in Fig. 1.

Since drainage holes (Fig. 3b) and sample positions are arranged alternately, space experiments in all five sample positions can be completed by moving the platform in

one direction. The engineering states of the five positions is exactly the same, so the use of samples, image observing, and heating process can be mutual backups, which increases the chance of success for the colloidal evaporation experiments in space.

3 How to Control the Droplet in the Space

The manipulation of liquid drops under microgravity environment could be very promising in space applications, such as life support systems, waste water treatment, heat exchangers, machining biologics and pharmacy [25, 26]. Over the past two decades, a variety of microgravity experiments concerning growth and manipulation of liquid drops had been performed. Antar et al. performed drop coalescence experiments through two hypodermic needles which were contacted using manual force, allowing the drops to coalesce [27]. Savino et al. examined wetting and coalescence of silicone oil sessile drops formed over copper substrates using a cylindrical copper needle with a coaxial hole [28]. To investigate gravity effect on the contact angle and the drop interface shape, Brutin et al. created drops by injection through a hole of the substrate [29]. All these works had already led to major advances for the drop manipulation in space. However, these solutions were too complicated; furthermore, the drops couldn't be fully constrained, which was likely to be unstable under vibration or attitude adjustment of the spacecraft. A more simple and reliable technique was necessary for the control of liquid drops under the conditions of weightlessness.

3.1 *The Confined Substrate for Droplet Pinning*

Patterned substrates on the basis of wetting enhancement or wetting barrier were always designed to manipulate the drop in terrestrial condition [30–34]. For examples, Tenjimbayashi et al. introduced a liquid manipulation strategy to design dynamically hydrophobic and statically hydrophobic/hydrophilic patterned surfaces [35]. Dong and McCarthy described a method for preparing super-hydrophobic surfaces containing guiding lines that control water motion [36]. Draper et al. designed the patterned surface with a super-hydrophobic polymer coating for the manipulation of droplets within microfluidic channels [37]. Zhang et al. designed super-hydrophobic TiO₂ nanostructures for condensate micro-drop self-propelling [38]. Wu et al. designed Laplace pressure pattern based on conical morphology and wetting heterogeneity for micro-droplet manipulation [39]. These works illustrated that the patterning technology had excellent performance in drop manipulation under terrestrial condition. We might wonder whether it was feasible to expand this technology to space as well. In fact, the drops could be easily kept stable on a substrate under the gravity force on earth that has nothing to do with the surface modification of the substrate. However, in microgravity environment, gravitational effects were negligibly small and surface tension effects dominated the liquid

behavior [40], thus the liquid can climb along the wetting surface [41, 42], which might be easily to result in catastrophic effects in space. Therefore, the applicability of drop manipulation through modifying the surface wettability in microgravity environment was still a problem that await for proof.

The rough and the non-uniform wettability of the contact line anchored the border of the droplet, which is referred to as canthotaxis effect [43]. In addition, the particles within the droplet will accumulate at the contact line during evaporation, which could change the roughness and the wettability of the contact line and result in the self-pinning effect [44]. The sample substrate will be placed on the copper sample holder, composed of hydrophilic and hydrophobic areas. The round hydrophilic area is a quartz surface with a diameter of 5 mm, which is surrounded by a super-hydrophobic coating (SHOS150; Shunytech). As can be seen in Fig. 4a, the white part is the super-hydrophobic coating and the center part is the confined hydrophilic area. Figure 4b shows that the super-hydrophobic contact angle of the coating is about 150° , and its thickness is nearly $60\ \mu\text{m}$, as shown in Fig. 4c. The sample substrate could confine a droplet with extremely volume of $100\ \mu\text{L}$ within the hydrophilic area, and prevent it from floating away in the microgravity of space. The polystyrene colloidal microspheres, dispersed in super-pure water with a mean diameter of $2.2\ \mu\text{m}$ were purchased from Duke (5200A). The polystyrene colloidal suspension will be prepared by diluting the original solution to 0.1% (w/w) with demonized water.

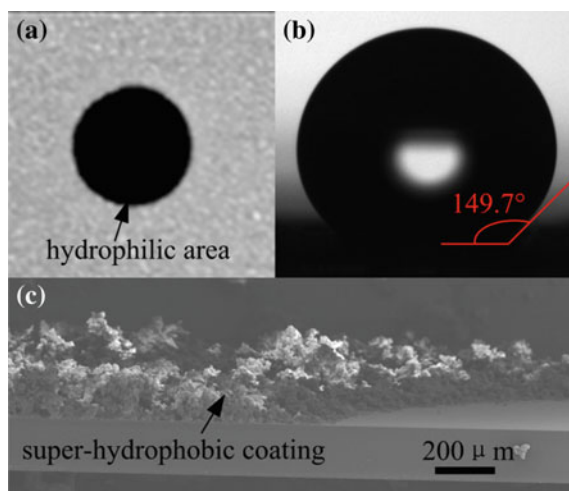


Fig. 4 Substrate with confined hydrophilic area. **a** A quartz crystal wafer with confined area treated by super-hydrophobic coating, the white part is the coating while the center part is the confined hydrophilic area; **b** The super-hydrophobic contact angle is about 150° ; **c** SEM image of the cross section of substrate shows that the thickness of the coating is nearly $60\ \mu\text{m}$. Reprinted from Ref. [24], copyright 2016, with permission from Springer

3.2 The Profiles of the Confined Colloidal Droplet on the Ground or in the Space

The drop shape was mainly dominated by two forces: the surface tension force, which tended to minimize the area of the surface to decrease the surface energy (producing typically a spherical shape), while the gravitational force which tended to flatten the drop. The balance of these two forces was described by the Bond number Bo , $Bo = (\rho_L - \rho_V)gL^2/\sigma$, where, ρ_L was the density of the liquid, ρ_V was the density of the vapor, L was the characteristic length, g was the gravitational acceleration, and σ was the liquid–vapor surface tension [45]. It was critical to choose the characteristic length.

The patterned substrate could be used for capturing water or water-based drops in space. The capture ability of the patterned substrate was attributed to its surface wettability. Evaporation studies were useful in characterizing wetting behavior because drops with various sizes can be created to evaluate the transition criterion [46, 47]. For a large drop resting on an ideal patterned substrate, with the decrease of the drop volume (V) as evaporation, three different regimes could be distinguished, as shown in Fig. 5a [48]. The intrinsic contact angles, which was determined by the chemical compositions, were θ_α and θ_β for α phase (hydrophobic region) and β phase (hydrophilic region), respectively. In regime 1 and 3, the apparent contact angle (ACA) was equal to the intrinsic contact angles. Different chemical compositions determined the wetting barrier at the interphase boundary between the hydrophilic region and the hydrophobic region. At this wetting barrier, the liquid surface turned from the contact angle with the better-wetting face to the contact angle with the worse-wetting face [49]. Therefore, in regime 2, the contact radius kept constant as R and the apparent contact angle (ACA) was in a closed interval $[\theta_\beta, \theta_\alpha]$. Thus, the aqueous drop of the specific volume in between $[V(R, \theta_\beta), V(R, \theta_\alpha)]$ could be pinned and constrained by the wetting barrier in this regime, which was responsible for the drop capturing. The super-wettable surfaces (α phase was super-hydrophobic, and the β phase was super-hydrophilic) could be chosen to achieve large drop capturing.

Figure 5a showed ideal homogeneous surfaces (α phase and β phase) that contact angle hysteresis (CAH) was negligible. In fact, the hysteresis could arise from any surface roughness or heterogeneity. We could speculate that the range of ACA in regime 2 would be wider for real surfaces, i.e., the maximum and minimum ACA were equal to the advancing contact angle of α phase and the receding contact angle of β phase. The advancing contact angle and receding contact angle for α phase and β phase could be marked as $\theta_{\alpha a}$, $\theta_{\alpha r}$, $\theta_{\beta a}$ and $\theta_{\beta r}$ in sequence. Thus, the ACA was in a closed interval $[\theta_{\beta r}, \theta_{\alpha a}]$ in regime 2. The volume of aqueous drop that could be constrained was in between $[V(R, \theta_{\beta r}), V(R, \theta_{\alpha a})]$, which was larger than the ideal patterned surface. In our experiment, the quartz glass and SHOS150 coating could be considered as α phase and β phase, respectively. We had measured the contact angles and hysteresis for water and water-based suspension on these two surfaces, as shown in Table 1. The aqueous drop with ACA between 26° and 156° could be constrained. For water-based suspension drop, the ACA was in between 17° and 137° . It was

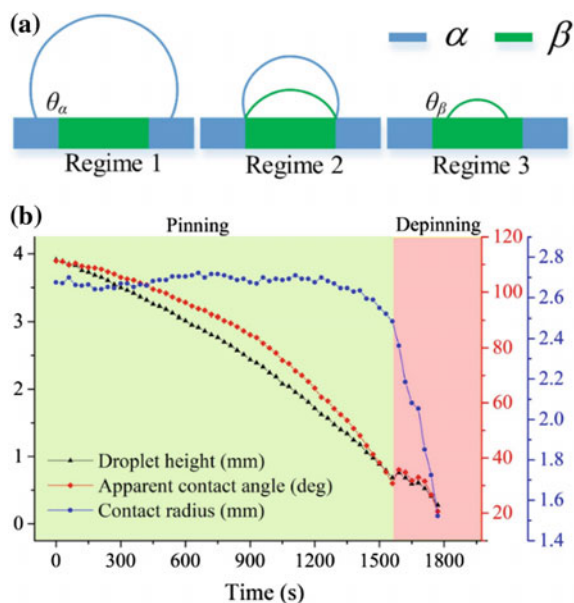


Fig. 5 **a** The three wetting regimes of a drop on the ideal patterned substrate as with evaporation, where the intrinsic contact angles are θ_α and θ_β in regimes 1 and 3, respectively. The drop could be confined in regime 2. **b** Evaporation of an aqueous drop on a patterned substrate with initial volume of $60 \mu\text{L}$ under microgravity environment. The black, red, and blue line represent the drop height, the apparent contact angle, and the contact radius variation versus time t , respectively. Reprinted from Ref. [50], copyright 2018, with permission from American Chemical Society

Table 1 Contact angles and hysteresis for water and water-based suspension on homogeneous surfaces, reprinted from Ref. [50], copyright 2018, with permission from American Chemical Society

Surfaces	Contact liquids					
	Water			Water-based suspension		
	θ_a (deg)	θ_r (deg)	$\Delta\theta$ (deg)	θ_a (deg)	θ_r (deg)	$\Delta\theta$ (deg)
Quartz glass	$62^\circ \pm 2^\circ$	$26^\circ \pm 2^\circ$	$36^\circ \pm 4^\circ$	$58^\circ \pm 3^\circ$	$17^\circ \pm 1^\circ$	$41^\circ \pm 4^\circ$
SHOS150 coating	$156^\circ \pm 2^\circ$	$134^\circ \pm 3^\circ$	$22^\circ \pm 5^\circ$	$137^\circ \pm 3^\circ$	$131^\circ \pm 3^\circ$	$6^\circ \pm 6^\circ$

Notes θ_a is the advancing contact angle, θ_r is the receding contact angle, and $\Delta\theta = \theta_a - \theta_r$ is the contact angle hysteresis of homogeneous surface

realized that the contact angles for water-based suspension were less than the purity water, which could be attributed to the decrease the surface energy of the aqueous solution because of impurities (PS microspheres).

The aqueous drops in regime 2 came in different shapes in space and on the ground, which meant that the drop volumes that could be captured by the patterned substrate might be unequal under the normal gravity and microgravity. We had further studied

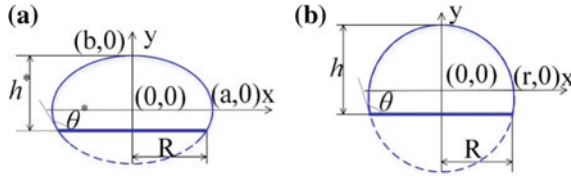


Fig. 6 **a** Geometry of an ellipsoidal cap-shaped drop model; **b** A spherical cap-shaped drop model. Reprinted from Ref. [50], copyright 2018, with permission from American Chemical Society

the gravity effect on the capacity of the substrate. The drop resting on the substrate on earth could be easily distorted by gravity, its shape could be considered as an oblate ellipsoidal cap geometry [51], where h^* was the drop height, θ^* was the ACA, R was the contact radius, as shown in Fig. 6a. The eccentricity value, e , was held constant for all times. The volume of the oblate ellipsoidal cap geometry was given by

$$V^* = \frac{\pi}{6(1 - e^2)} [3(1 - e^2)R^2 + h^{*2}]h^* \tag{1}$$

The ACA of the drop could be expressed as

$$\theta^* = \arctan\left[\frac{2h^*R(1 - e^2)}{(1 - e^2)R^2 - h^{*2}}\right] (1 > e \geq 0) \tag{2}$$

For a drop in microgravity condition, it could be considered having the shape of a spherical cap, as shown in Fig. 6b. The drop volume V could be expressed as a function of the contact radius R , and the ACA,

$$V(R, \theta) = \frac{\pi R^3}{3} \frac{(1 - \cos \theta)^2(2 + \cos \theta)}{\sin^3 \theta} \tag{3}$$

The ACA could be expressed as a function of the drop height h and the contact radius R ,

$$\theta = 2 \arctan \frac{h}{R} \tag{4}$$

3.3 The Evaporation of the Droplet in the Space

To reveal the confinement mechanism of the substrate, evaporation experiments of water drops with different initial volumes (30, 40, 50, 60, 70 μL) had been conducted under microgravity conditions. A typical drop with initial volume of 60 μL was chosen to describe the wetting transition. The time evolution of the drop height, the ACA, and the contact radius, were shown in Fig. 5b. The evaporation process

could be divided into two stages. In the first stage, the height and the ACA of the drop nonlinearly decreased with time, but in the meanwhile, the contact radius kept unchanged, and the drop evaporated in constant contact radius (CCR) mode. The drop evaporation spends almost all of its time in this stage, which could be characterized by the quasi-steady diffusion-driven evaporation model. In the last minute of evaporation, the contact line began to slip suddenly and the evaporation entered into the second stage. We noted that the ACA at the transition point (30.8°) was nearly equal to the receding contact angle of the quartz glass (26°), which fitted basically with the theoretical prediction. In the second stage, the contact radius decreased rapidly, the height and the ACA showed a broken line variation, and the drop evaporated as a skip-slip mode. What we cared about was the first stage of evaporation, which corresponded to regime 2. For water-based suspension drop, the ACA at the transition point ($\sim 17^\circ$) was less than the water drop's (26°). Actually, there was no transition point for an evaporating colloidal drop, because a ring-like stain formed near the contact line, which enhanced the pinning effect and made the drop evaporating as CCR mode. The surface irregularities and unevenness of the patterned substrate was inevitable in our experiment, which would enhance the pinning effect and make the drop being confined more firmly.

The drop was considered to be equivalent to the spherical drop with the same volume, and we chose the diameter of this spherical drop as the characteristic length, thus the Bond number (Bo) of the drops with different equivalent volumes (V_e) in normal gravity could be calculated. The differences of the ACA ($\Delta\theta = \theta^* - \theta$) and the height ($\Delta h = h - h^*$) of the drop between normal gravity and microgravity were plotted versus the Bond number, as shown in Fig. 7d. $\Delta\theta$ and Δh could be used to judge the shape deviation of the drop in normal gravity from an ideal spherical cap drop in microgravity. When the $Bo < 1$ ($V_e < 10.3 \mu\text{L}$), $\Delta\theta$ and Δh was close to zero, which meant that the drop shape could be hardly affected by gravity. When the $Bo = 1$ ($V_e = 10.3 \mu\text{L}$), the characteristic length $L = 2.7 \text{ mm}$ (the capillary length), the equivalent volume of the drop was $10.3 \mu\text{L}$, which coincided with the experimental results ($10 \mu\text{L}$), as shown in Fig. 7c. When the $Bo > 1$ ($V_e = 10.3 \mu\text{L}$), $\Delta\theta$ and Δh increased as with increasing of the Bond number, so the flattening effect of the drop resulting from gravity was more pronounced for higher values of the Bond number. It indicated that the ACA could be easier to reach to the advancing contact angle of the hydrophobic region for drops in normal gravity, so this patterned substrate could confine drops with greater volume in space than on earth. Therefore, the gravity effect significantly influenced the confinement capacity of the patterned substrate, the bigger the drop volume, the larger the gravity effect on its confinement capacity.

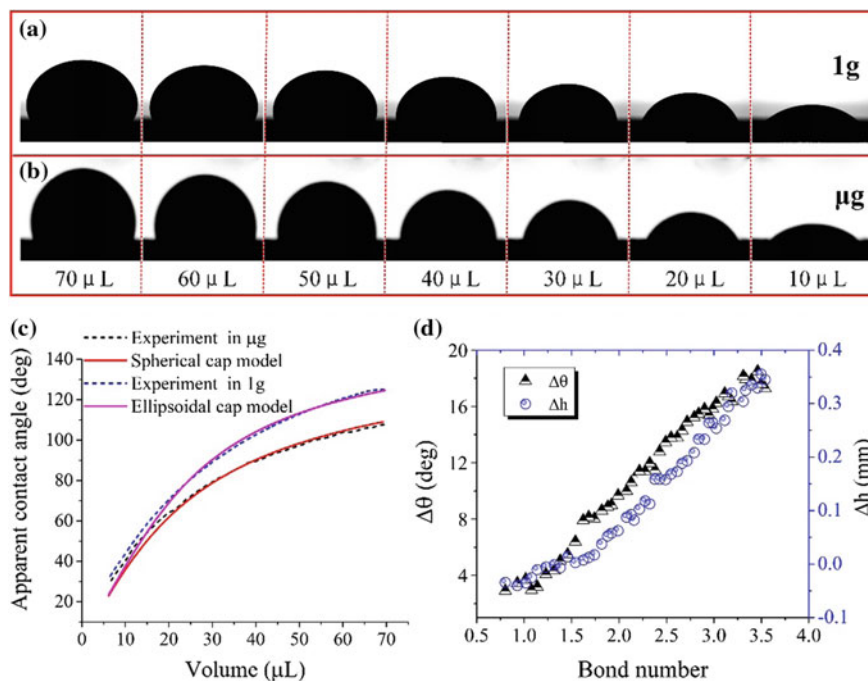


Fig. 7 Profile images of drop with different volume at normal gravity (a) and microgravity (b) conditions during the evaporation process; c The theoretical and experimental apparent contact angles were plotted versus volume for evaporating drops in normal gravity and microgravity ($e = 0.56$); d The differences of the apparent contact angle ($\Delta\theta$) and the height (Δh) of the drop between normal gravity and microgravity were plotted versus the Bond number (Bo). Reprinted from Ref. [50], copyright 2018, with permission from American Chemical Society

4 The Self-assembly of the Colloidal Particles

4.1 Multi-physical Effects During the Droplet Evaporation

The evaporation of a sessile colloidal droplet occurs commonly in nature, and the evaporation process involves multiple physical phenomenon including pinning effects [52, 53], convection flow [52, 53], dewetting [54], and capillary forces [55, 56]. These physical effects influence a wide range of applications, such as photonic crystal formation [57], nano-material assembly [58], injection printing [59], and biotechnology [60, 61]. When the contact angle is small, the evaporation will induce the outward capillary flow mainly which bring the particles to the edge, eventually forming the familiar “coffee-ring” pattern [62]. As far as applications are concerned, the most important thing is to know how the deposition morphologies form and then how to control the deposition pattern. During droplet evaporation, surfactant [63] or a temperature gradient [64] along the droplet surface induced Marangoni flow,

which could affect the flow field and the distribution of particles on the substrate, but it was the only element to determine the ultimate patterns. It was found that minimizing contact angle hysteresis could lead to the formation of a central stain, rather than a ring [65, 66]. Particles that spontaneously adsorb at the substrate [67] or migrate at the liquid–vapor interface [68] also oppose the coffee ring effect. Even in the presence of pinning, the ring formation can be impeded by the presence of a reverse (i.e. inward) flow during evaporation [44, 69], which can be caused by a temperature-driven or surfactant-induced Marangoni effect [64, 70]. Even the shape of the particles can lead a different deposition process [71].

The works above might have created an impression that the final pattern morphologies were determined by various flows inside the droplet. However, in the final stage of evaporation, the pinned droplet evolves into a thin liquid film, which spontaneously undergoes dewetting and promotes particles redistribution to form the resulting patterns inside the coffee ring.

Recently, significant progress had been made in understanding the dewetting process of liquid film [72]. In the absence of particles, two different film rupture mechanisms have been identified that occur in film of nanoscale thickness, nucleation dewetting and spinodal dewetting [73–75]. The formation of characteristic patterns such as annular ring-like structures [76] and dendritic structure [77] by dewetting of thin film have been analyzed in liquid film that contains particles. In previous studies, the focus is on the dewetting of ultrathin films with or without nanoparticles, which provide a rapid, bottom-up approach to create textures on a surface [78, 79]. Compared with nanoscale liquid film, micro-sized film is more stable, and may more easily allow the assembly of particles into ordered structures, especially a close-packed hexagonal structure. However, the dewetting process of micro-sized film containing microspheres still remains unclear, though it is involved in the final stages of evaporation of most colloidal drops. The film stability–instability (rupture) is the subject of thermal–mechanical and capillary surface waves caused by spatial variations of the surface tension due to the temperature or surfactant concentration.

4.2 The Effect of the Gravity for the Deposition Pattern

The most common phenomenon is the coffee-ring effect, which was attributed to the outward capillary flow caused by the uneven evaporation flux, on the conditions of the droplet evaporating in constant contact radius (CCR) mode at a small contact angle. The capillary flow will bring the suspended particles from the center to the edge of the droplet, and these particles will accumulate near the contact line and finally form the ring-like stain. In contrast, the presence of Marangoni flow, induced by temperature gradients or concentration gradient on the droplet surface, could reverse the capillary flow and change the deposition patterns [64, 69, 70, 80]. In addition, particles will be inevitably affected by the gravitational effect in the process of droplet evaporation on the ground. It was demonstrated that gravity has a significant influence on deposition patterns [81, 82]. Further studies show that the deposition

profiles could be determined by the capillary forces [83], liquid film dewetting [84], and interface capture [85].

In fact, the above-mentioned phenomena are frequently involved in the droplet evaporation process at the same time, which will cooperate or compete together. The final deposition morphology could be determined by these two or more effects. In the past, the deposition morphology which were determined by the interaction between the coffee ring effect and other phenomenon, such as Marangoni effect, shape-dependent capillary interactions, capillary force, contact angle hysteresis, were widely reported [68, 86–88]. Despite great progress, to our best knowledge, there are still no studies that examine the combined effects of the coffee ring and gravity sedimentation on deposition patterns.

For the differences of deposition patterns between sessile and pendant droplet is the gravity effect, which can be described by the gravitational Peclet number. The Peclet number is defined as:

$$Pe_G = \frac{\pi d^4 g \Delta\rho}{12k_B T} \quad (5)$$

where d is the particle diameter, $\Delta\rho$ is the difference in density between the particles and the surrounding fluid, g is the gravitational acceleration, k_B is the Boltzmann constant, and T is the temperature. The smaller particles have a lower Peclet number, and thus follow the streamlines closely, but the larger particles can be easily pulled downward by gravity.

For both sessile and pendant droplet with a lower Peclet number, the gravity sedimentation is weak, thereby most particles still exist inside the droplet when the contact angle is small in the final stage of evaporation, which will be taken by the capillary flow towards the edge and finally formed the ring-like stain.

4.3 The Mechanism for Encounter and Pursuit

The interface shrinkage, the gravitational sedimentation and the capillary flow in different stages of evaporation. For an evaporating droplet, the terminal velocity of sphere falling in a fluid can be described by the Stokes law [89]:

$$u_p = \frac{d^2 \Delta\rho g}{18\eta} \quad (6)$$

where u_p is the terminal velocity, d the particles diameter, η is the viscosity, g is the gravitational constant, $\Delta\rho$ is the difference in density of the particle and the dispersed phase. As the particle size increases, the sedimentation rate increases and the particles will settle faster.

The average interface shrinkage rate could be expressed as follows:

$$u_i = \frac{h}{t_f} \quad (7)$$

where h is the initial height of the droplet, t_f is the final evaporation time, which can be calculated if the droplet evaporation is considered as the quasi-steady, diffusion-driven evaporation model [90]. The average interface shrinkage rate is determined by the droplet shape and the evaporation rate.

The capillary flow, which is caused by the uneven evaporation flux of the droplet surface, could take particles from the center to the edge. Close to the contact line, the height-averaged radial velocity u_c can be expressed by equation [91]:

$$u_c = \frac{D^*}{\theta} \frac{1}{\sqrt{R(R-r)}} \quad (8)$$

where D^* is the diffusion coefficient, R is the contact radius of the drop, r is the distance from the drop center, θ is the contact angle. There is an inverse correlation between the velocity of the capillary flow and the contact angle. As mentioned earlier, the droplet evaporates as CCR mode, thereby the contact angle decreases continuously. Therefore, the capillary flow enhanced in the evaporation process.

The competitive effect between the radial velocity and the terminal velocity can be described as the dimensionless group number from Eqs. (6) and (8):

$$u_p/u_c = \frac{\Delta\rho g \sqrt{R(R-r)}}{18\eta D^*} d^2\theta \quad (9)$$

The velocity ratio of the interface shrinkage rate and the radial velocity can be expressed through Eqs. (7) and (8)

$$u_i/u_c = \frac{\sqrt{R(R-r)} h\theta}{D^* t_f} \quad (10)$$

The particle deposition in an evaporating droplet can be divided into two stages. In the first stage, the contact angle is large enough and the capillary flow is weak to be negligible. There are two different regimes for sessile and pendant droplets in this stage: the pursuit regime and the meeting regime, as shown in Fig. 8. In the pursuit regime, both the direction of the interface shrinkage and the particle sedimentation are downward, it seems like that the descending interface is pursuing the particles. If $u_p > u_i$, the particles fall fast and never meet with the liquid–air interface. Thus, parts of particles fall directly on the substrate and the rest particles remain inside the droplet. If $u_p < u_i$, the interface is able to catch up with particles and capture them. Then one part of these particles accumulates at the interface, the other part remains inside the droplet. In the meeting regime, the direction of the interface shrinkage and the particle sedimentation is opposite, it seems like that the ascending interface tends to meet with the particles. If the value $|u_p u_i|$ is large, the interface will meet with particles and capture them, nearly all of particles will assemble monolayer islands at

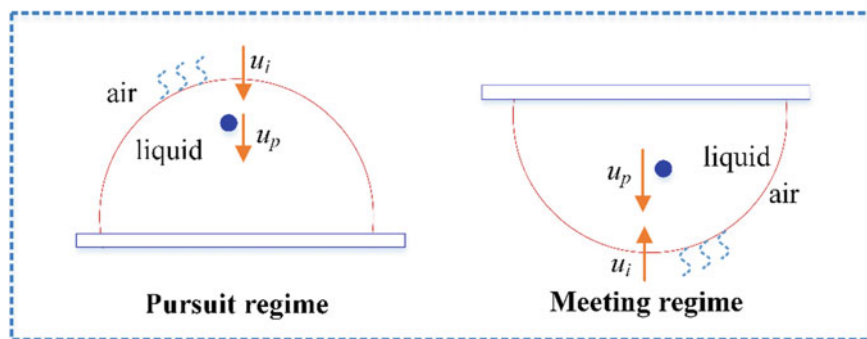


Fig. 8 Schematic of the pursuit regime and the meeting regime for sessile droplet and pendant droplet, respectively. Reprinted from Ref. [92], copyright 2019, with permission from American Chemical Society

the interface. If the value $|u_p u_i|$ is small, the interface will hardly encounter particles, thus most of particles remain inside the droplet. It is worth mentioning that these particles close to the liquid–air interface may be acceleratedly captured under the effect of recirculation flow. In the second stage, the contact angle is small and the outward capillary flow dominates the particles motion. If there are enough particles inside the droplet, these particles will be taken to the edge and form ring-like stain. Otherwise, for the particles being trapped at the liquid–air interface, they will transfer directly to the substrate and form centered stain. These theories mentioned above can explain the deposition patterns for both sessile and pendant droplet containing different particles well.

5 Conclusion and Outlook

In this chapter, we have introduced a method for capturing colloidal drops in space based on patterned substrate, and further studied the deposition behavior of colloidal particles inside the drop. The space experiments demonstrate how capillary forces work in space, how the patterned surface change the wetting behavior and achieve the manipulation of an aqueous drop, and how a constrained drop evaporates in space. The patterns formation of evaporating constrained drops containing particles has been investigated. It was found a network pattern formed inside the coffee ring. Results show that there is a complex and strong interplay between liquid film dewetting and particle aggregation: the non-uniform distribution of particles promotes the rupture of the liquid film and the liquid film in turn dominates the particle assembly process. We reported the interactions of different physical effects through drying sessile and pendant droplets and found that the deposition morphology is the result of competition and cooperation interactions of the free setting, the interface shrinkage and the outward capillary flow.

As we know, interest in wetting has increased enormously over the last two decades, particularly since 2010. This growth can be attributed to increasing interest of scientists worldwide to capillarity and wetting phenomena, which is caused by their wider application to various new areas. Understanding how microgravity amplifies the wetting behaviors could improve the reliability of such key processes as liquid fuel storage and supply, and general liquid transport aboard spacecraft. Some fluid handling processes in space are prone to involve complex fluids, such as colloidal suspension, emulsions and biological fluids. The microgravity environment may greatly influence the physical behavior of these complex fluids. A good knowledge of the mechanisms involved can help engineers to predict the behavior of complex fluids, and factor that into the design of space systems.

The wetting and evaporation of a colloidal drop attracts more many researchers' interests after the "coffee ring" effect found by Deegan since 1997. However, for the most part, asystematic, well-established, body of knowledge on deposition from drying droplets is not yet available. Future works are expected to study on the relationship between the macroscopic droplet shape and microscopic particle deposition, the underlying mechanisms of evaporation-induced changes of the local flow field, as well as the control of the "coffee ring" effect and the specific deposition patterns.

It would be nice to see the patterns from drying drops of complex fluids used for the early diagnosis of patients since it is a cheap and simple method. However, the understanding of mechanisms behind patterns left from complex fluids is still lacking. In addition, biological fluids are incredibly complex, containing numerous different materials that interact with each other to create very complicated patterns and make them very difficult to model. Finally, the gravity effect on the patterns formation of human body fluid is still unclear, which need to clarify under microgravity conditions. The patterns left from drops of human body fluid of similar condition should be regularly recorded under space and terrestrial conditions. With the increase in repeatable patterns, it can be hoped that this technique will be used to diagnose health status of astronaut.

References

1. Cao H, Lan D, Wang Y, Volinsky AA, Duan L, Jiang H (2010) Fracture of colloidal single-crystal films fabricated by controlled vertical drying deposition. *Phys Rev E* 82(3):031602
2. Schall P, Cohen I, Weitz DA, Spaepen F (2004) Visualization of dislocation dynamics in colloidal crystals. *Science* 305(5692):1944–1948
3. Pusey P, Van Megen W (1986) Phase behaviour of concentrated suspensions of nearly hard colloidal spheres. *Nature* 320(6060):340–342
4. Lin Z (2012) *Evaporative self-assembly of ordered complex structures*. World Scientific
5. Yin Y, Lu Y, Gates B, Xia Y (2001) Template-assisted self-assembly: a practical route to complex aggregates of monodispersed colloids with well-defined sizes, shapes, and structures. *J Am Chem Soc* 123(36):8718–8729
6. Norris DJ, Arlinghaus EG, Meng L, Heiny R, Scriven L (2004) Opaline photonic crystals: how does self-assembly work? *Adv Mater* 16(16):1393–1399

7. Deegan RD, Bakajin O, Dupont TF, Huber G, Nagel SR, Witten TA (1997) Capillary flow as the cause of ring stains from dried liquid drops. *Nature* 389(6653):827–829
8. Hampton MA, Nguyen TA, Nguyen AV, Xu ZP, Huang L, Rudolph V (2012) Influence of surface orientation on the organization of nanoparticles in drying nanofluid droplets. *J Colloid Interface Sci* 377(1):456–462
9. Van Blaaderen A, Ruel R, Wiltzius P (1997) Template-directed colloidal crystallization. *Nature* 385(6614):321–324
10. Dag Ö, Ahari H, Coombs N, Jiang T, Aroca-Ouellette PP, Petrov S, Sokolov I, Verma A, Vovk G, Young D (1997) Does microgravity influence self-assembly? *Adv Mater* 9(15):1133–1149
11. Priestly E (2012) Introduction to liquid crystals. Springer Science & Business Media
12. Onsager L (1949) The effects of shape on the interaction of colloidal particles. *Ann N Y Acad Sci* 51(4):627–659
13. Frenkel D (1987) Onsager's spherocylinders revisited. *J Phys Chem* 91(19):4912–4916
14. Baulin VA (2003) Self-assembled aggregates in the gravitational field: growth and nematic order. *J Chem Phys* 119(5):2874–2885
15. Murai M, Okuzono T, Yamamoto M, Toyotama A, Yamanaka J (2012) Gravitational compression dynamics of charged colloidal crystals. *J Colloid Interface Sci* 370(1):39–45
16. Okubo T, Tsuchida A, Okuda T, Fujitsuna K, Ishikawa M, Morita T, Tada T (1999) Kinetic analyses of colloidal crystallization in microgravity-aircraft experiments. *Colloids Surf, A* 153(1):515–524
17. Cheng Z, Zhu J, Russel WB, Meyer WV, Chaikin PM (2001) Colloidal hard-sphere crystallization kinetics in microgravity and normal gravity. *Appl Opt* 40(24):4146–4151
18. Ansari RR, Hovenac EA, Sankaran S, Koudelka JM, Weitz DA, Cipelletti L, Segre PN (1999) Physics of colloids in space experiment. In: *Space technology and applications international forum-1999*, vol 1. AIP Publishing, pp 108–113
19. Okubo T, Tsuchida A, Takahashi S, Taguchi K, Ishikawa M (2000) Kinetics of colloidal alloy crystallization of binary mixtures of monodispersed polystyrene and/or colloidal silica spheres having different sizes and densities in microgravity using aircraft. *Colloid Polym Sci* 278(3):202–210
20. Schöpe HJ, Wette P (2011) Seed- and wall-induced heterogeneous nucleation in charged colloidal model systems under microgravity. *Phys Rev E* 83(5):051405
21. Hu W (2008) Special issue: microgravity experiments on board the Chinese recoverable satellites preface. In: *Springer 233 Spring St, New York, NY, USA*
22. Li C, Zhao H, Ni R (2008) China's recoverable satellites and their onboard experiments. *Microgravity Sci Technol* 20(2):61–65
23. Hu W, Zhao J, Long M, Zhang X, Liu Q, Hou M, Kang Q, Wang Y, Xu S, Kong W (2014) Space program SJ-10 of microgravity research. *Microgravity Sci Technol* 26(3):159–169
24. Li W, Lan D, Sun Z, Geng B, Wang X, Tian W, Zhai G, Wang Y (2016) Colloidal material box: in-situ observations on colloidal self-assembling and liquid phase transition in space. *Microgravity Sci Technol* 28(2):179–188
25. Conrath M, Canfield P, Bronowicki P, Dreyer ME, Weislogel MM, Grah A (2013) Capillary channel flow experiments aboard the International Space Station. *Phys Rev E* 88(6):063009
26. Bostwick J, Steen P (2015) Stability of constrained capillary surfaces. *Annu Rev Fluid Mech* 47:539–568
27. Antar BN, Ethridge EC, Maxwell D (2003) Viscosity measurement using drop coalescence in microgravity. *Microgravity Sci Technol* 14(1):9–19
28. Savino R, Nota F, Fico S (2003) Wetting and coalescence prevention of drops in a liquid matrix. Ground and parabolic flight results. *Microgravity Sci Technol* 14(3):3–12
29. Brutin D, Zhu Z, Rahli O, Xie J, Liu Q, Tadrist L (2009) Sessile drop in microgravity: creation, contact angle and interface. *Microgravity Sci Technol* 21(1):67–76
30. Nakajima A (2011) Design of hydrophobic surfaces for liquid droplet control. *NPG Asia Materials* 3:49
31. Bormashenko E (2015) Progress in understanding wetting transitions on rough surfaces. *Adv Coll Interface Sci* 222:92–103

32. Herminghaus S, Brinkmann M, Seemann R (2008) Wetting and dewetting of complex surface geometries. *Annu Rev Mater Res* 38:101–121
33. Zhao XD, Fan HM, Liu XY, Pan H, Xu HY (2011) Pattern-dependent tunable adhesion of superhydrophobic MnO₂ nanostructured film. *Langmuir* 27(7):3224–3228
34. Lai Y, Pan F, Xu C, Fuchs H, Chi L (2013) In situ surface-modification-induced superhydrophobic patterns with reversible wettability and adhesion. *Adv Mater* 25(12):1682–1686
35. Tenjimbayashi M, Higashi M, Yamazaki T, Takenaka I, Matsubayashi T, Moriya T, Komine M, Yoshikawa R, Manabe K, Shiratori S (2017) Droplet motion control on dynamically hydrophobic patterned surfaces as multifunctional liquid manipulators. *ACS Appl Mater Interfaces* 9(12):10371–10377
36. Dong T, McCarthy TJ (2017) Superhydrophobic, low-hysteresis patterning chemistry for water-drop manipulation. *ACS Appl Mater Interfaces* 9(47):41126–41130
37. Draper MC, Crick CR, Orlickaite V, Turek VA, Parkin IP, Edel JB (2013) Superhydrophobic surfaces as an on-chip microfluidic toolkit for total droplet control. *Anal Chem* 85(11):5405–5410
38. Zhang S, Huang J, Tang Y, Li S, Ge M, Chen Z, Zhang K, Lai Y (2017) Understanding the role of dynamic wettability for condensate microdrop self-propelling based on designed superhydrophobic TiO₂ nanostructures. *Small* 13(4)
39. Wu L, Dong Z, Li F, Song Y (2018) Designing laplace pressure pattern for microdroplet manipulation. *Langmuir* 34(2):639–645
40. Stange M, Dreyer ME, Rath HJ (2003) Capillary driven flow in circular cylindrical tubes. *Phys Fluids* 15(9):2587–2601
41. Dreyer M, Delgado A, Path H-J (1994) Capillary rise of liquid between parallel plates under microgravity. *J Colloid Interface Sci* 163(1):158–168
42. Wang C-X, Xu S-H, Sun Z-W, Hu W-R (2010) A study of the influence of initial liquid volume on the capillary flow in an interior corner under microgravity. *Int J Heat Mass Transf* 53(9):1801–1807
43. Ondarçuhu T, Veyssié M (1991) *J Phys II* 1:75
44. Weon BM, Je JH (2013) *Phys Rev Lett* 110:028303
45. Diana A, Castillo M, Brutin D, Steinberg T (2012) Sessile drop wettability in normal and reduced gravity. *Microgravity Sci Technol* 24(3):195–202
46. Tsai P, Lammertink RG, Wessling M, Lohse D (2010) Evaporation-triggered wetting transition for water droplets upon hydrophobic microstructures. *Phys Rev Lett* 104(11):116102
47. Jung YC, Bhushan B (2007) Wetting transition of water droplets on superhydrophobic patterned surfaces. *Scr Mater* 57(12):1057–1060
48. Lenz P, Lipowsky R (1998) Morphological transitions of wetting layers on structured surfaces. *Phys Rev Lett* 80(9):1920
49. Langbein D (2002) Canthotaxis/wetting barriers/pinning lines. *Capill Surf* 149–177
50. Li W, Lan D, Sun H, Wang Y (2018) Drop capturing based on patterned substrate in space. *Langmuir* 34(16):4715–4721
51. Erbil HY, Meric RA (1997) Evaporation of sessile drops on polymer surfaces: ellipsoidal cap geometry. *J Phys Chem B* 101(35):6867–6873
52. Han W, Lin Z (2012) *Angew Chem Int Ed* 51:1534
53. Larson RG (2014) *AIChE J* 60:1538
54. Stannard A (2011) *J Phys: Condens Matter* 23:083001
55. Kralchevsky PA, Denkov ND (2001) *Curr Opin Colloid Interface Sci* 6:383
56. Xu J, Xia J, Hong SW, Lin Z, Qiu F, Yang Y (2006) *Phys Rev Lett* 96:066104
57. Norris DJ, Arlinghaus EG, Meng L, Heiny R, Scriven L (2004) *Adv Mater* 16:1393
58. Xie Y et al (2013) *Langmuir* 29:6232
59. Shimon A, Azoubel S, Magdassi S (2014) *Nanoscale* 6:11084
60. Wong T-S, Chen T-H, Shen X, Ho C-M (2011) *Anal Chem* 83:1871
61. Askounis A, Takata Y, Sefiane K, Koutsos V, Shanahan ME (2016) *Langmuir* 32:4361
62. Deegan RD, Bakajin O, Dupont TF, Huber G, Nagel SR, Witten TA (1997) *Nature* 389:827
63. Marin A, Liepelt R, Rossi M, Kähler CJ (2016) *Soft Matter* 12:1593
64. Hu H, Larson RG (2006) *J Phys Chem B* 110:7090

65. Eral HB, Augustine DM, Duits MHG, Mugele F (2011) *Soft Matter* 7:4954–4958
66. Lafuma A, Quéré D (2011) *EPL* 96:56001
67. Crivoi A, Duan F (2013) *Langmuir* 29:12067–12074
68. Yunker PJ, Still T, Lohr MA, Yodh AG (2011) *Nature* 476:308–311
69. Hu H, Larson RG (2005) *Langmuir* 21:3972–3980
70. Still T, Yunker PJ, Yodh AG (2012) *Langmuir* 28:4984–4988
71. Yunker P, Still T, Lohr M, Yodh A (2011) *Nature* 476(7360):308–311
72. Nikolov A, Wasan D (2014) *Adv Coll Interface Sci* 206:207
73. Reiter G (1992) *Phys Rev Lett* 68:75
74. Elbaum M, Lipson S (1994) *Phys Rev Lett* 72:3562
75. Thiele U, Mertig M, Pompe W (1998) *Phys Rev Lett* 80:2869
76. Ohara PC, Gelbart WM (1998) *Langmuir* 14:3418
77. Harrington GF, Campbell JM, Christenson HK (2013) *Cryst Growth Des* 13:5062
78. Rezende CA, Lee L-T, Galembeck F (2007) *Langmuir* 23:2824
79. Gentili D, Foschi G, Valle F, Cavallini M, Biscarini F (2012) *Chem Soc Rev* 41:4430
80. Girard F, Antoni M, Sefiane K (2008) *Langmuir* 24:9207–9210
81. Sandu I, Fleaca CT (2011) *J Colloid Interface Sci* 358:621–625
82. Devlin NR, Loehr K, Harris MT (2016) *AIChE J* 62:947–955
83. Weon BM, Je JH (2010) *Phys Rev E* 82:015305
84. Li W, Lan D, Wang Y (2017) *Phys Rev E* 95:042607
85. Li Y, Yang Q, Li M, Song Y (2016) *Sci Rep* 6
86. Majumder M, Rendall CS, Eukel JA, Wang JY, Behabtu N, Pint CL, Liu T-Y, Orbaek AW, Mirri F, Nam J (2012) *J Phys Chem B* 116:6536–6542
87. Weon BM, Je JH (2013) *Phys Rev E* 87:013003
88. Li Y-F, Sheng Y-J, Tsao H-K (2013) *Langmuir* 29:7802–7811
89. Rhodes MJ (2008) *Introduction to particle technology*. Wiley
90. Sobac B, Brutin D (2012) Thermal effects of the substrate on water droplet evaporation. *Phys Rev E* 86(2):021602
91. Marín ÁG, Gelderblom H, Lohse D, Snoeijer JH (2011) Order-to-disorder transition in ring-shaped colloidal stains. *Phys Rev Lett* 107(8):085502
92. Li W, Ji W, Sun H, Lan D, Wang Y (2019) Patterns formation in drying sessile and pendant droplet: interactions of gravity settling, interface shrinkage and capillary flow. *Langmuir* 35(1):113–119